Quantum noise of a harmonic oscillator under classical feedback control*

Feng Tang(汤丰) and Nan Zhao(赵楠)†

Beijing Computational Science Research Center, Beijing 100193, *China*

(Received 6 April 2020; revised manuscript received 25 June 2020; accepted manuscript online 15 July 2020)

Quantum sensing has been receiving researcher's attention these years due to its ultrahigh sensitivity and precision. However, the bandwidth of the sensors may be low, thus limiting the scope of their practical applications. The low-bandwidth problem is conquered by feedback control methods, which are widely utilized in classic control fields. Based on a quantum harmonic oscillator model operating near the resonant point, the bandwidth and sensitivity of the quantum sensor are analyzed. The results give two important conclusions: (a) the bandwidth and sensitivity are two incompatible performance parameters of the sensor, so there must be a trade-off between bandwidth and sensitivity in practical applications; (b) the quantum white noise affects the signal to be detected in a non-white form due to the feedback control.

Keywords: quantum sensing, feedback, sensitivity, bandwidth

PACS: 03.67.–a, 87.19.lr **DOI:** 10.1088/1674-1056/aba5fb

1. Introduction

Quantum sensing has emerged as a distinct and rapidly growing branch of research, which employs quantum mechanical systems as sensors to detect various physical quantities ranging from magnetic and electric fields, to time, frequency and rotations. Aiming at ultra-high sensitivity and precision, researchers have devised various of quantum sensors including atomic vapors sensors,[1–4] trapped ions sensors,[5–7] solid-state spins sensors,[8–11] and so on. By using quantum entanglement[12–14] and squeezing,[15–17] the sensitivity or precision of the quantum sensors have reached or even gone beyond the standard quantum limit, which is unreachable by classical measurement method. Undoubtedly, quantum sensing has opened a new door to the measurement areas.

The sensitivity of a quantum sensor scales as[18]

$$\text{sensitivity} \propto \frac{1}{\kappa\sqrt{T_\chi}}, \tag{1}$$

where κ is a transduction parameter related to the response of the quantum sensor to the signal to be measured, and T_χ is the coherence time of the quantum sensor. Better sensitivity requires longer coherence time besides a large transduction parameter. However, longer coherence time, which reflects greater immunity of the quantum sensor to its environment, indicates a narrower bandwidth of the sensor. This may be a intractable issue when applying the quantum sensors to practical applications.

A well-known method in classical control theory to increase the bandwidth of a dynamical system is to the close-loop feedback control. In this paper, a simple model based on the analysis of feedback control of a quantum sensor is presented to show the relationship between bandwidth and sensitivity. The results indicate that bandwidth and sensitivity are two competing factors of the quantum sensor, when intrinsic noise of the sensor system due to its quantum characteristics is taken into consideration. This means that there must be a trade-off between bandwidth and sensitivity of the quantum sensor system.

2. Model of the quantum sensor

In this section, we give a simple model revealing the basic physics underlying the operational principles of the quantum sensor. At the same time, this model shows an unconquerable sensitivity limit imposed by the quantum feature of the sensor. The Hamiltonians of the sensor and the environment read

$$H_0 = \hbar\omega_0 a^\dagger a + \hbar g\cos(\omega t)(a + a^\dagger), \tag{2}$$

$$H_{\text{bath}} = \hbar\sum_j \omega_j b_j^\dagger b_j, \tag{3}$$

$$H_{\text{I}} = \hbar\sum_j g_j(a^\dagger b_j + \text{h.c.}), \tag{4}$$

where H_0 describes a harmonic oscillator driven by a classical driving field with frequency ω and coupling strength g. The environment is modeled by an ensemble of harmonic oscillators with j specifying different oscillator mode. The interaction of the oscillator with its environment, H_{I}, will exert a fluctuating force on the oscillator, resulting in the dissipation of the harmonic oscillator.

The quantum Langevin equation for the harmonic oscillator is

$$\dot{a}(t) = -\text{i}\omega_0 a(t) - \text{i}g\cos(\omega t) - \frac{\gamma}{2}a(t) + f_{\text{a}}(t), \tag{5}$$

*Project supported by the National Natural Science Foundation of China (Grant Nos. 11534002, U1930402, and U1930403).

†Corresponding author. E-mail: nzhao@csrc.ac.cn

where

$$f_{\rm a}(t) = -{\rm i}\sum_j g_j b_j(0)\,{\rm e}^{-{\rm i}\omega_j t} \tag{6}$$

is the noise operator and $\gamma = 2\pi g^2(\omega_0)D(\omega_0)$ is the decay rate of the oscillator induced by the environment.[19] Here $D(\omega_0) = V\omega_0^2/\pi^2c^3$ is the density of the bath states at ω_0, V is the quantization volume and c is the velocity of light. Then the average values of the two quadrature amplitudes of the oscillator $X_1 = (a+a^\dagger)/2$ and $X_2 = (a-a^\dagger)/2{\rm i}$ follow the equations:

$$\begin{aligned}\langle\dot{X}_1\rangle &= \omega_0\langle X_2\rangle - \frac{\gamma}{2}\langle X_1\rangle,\\ \langle\dot{X}_2\rangle &= -\omega_0\langle X_1\rangle - \frac{\gamma}{2}\langle X_2\rangle - g\cos(\omega t).\end{aligned} \tag{7}$$

In deriving Eq. (7), the density operator of the composite system is assumed to be $\rho_{\rm c} = \rho_{\rm S}\otimes\rho_{\rm B}$ at $t = 0$, where the harmonic oscillator and the bath are both in the thermal states

$$\rho_{\rm S} = \frac{1}{Z_{\rm S}}\,{\rm e}^{-\frac{\hbar\omega_0 a^\dagger a}{k_{\rm B}T}}, \tag{8}$$

$$\rho_{\rm B} = \frac{1}{Z_{\rm B}}\,{\rm e}^{-\frac{H_{\rm bath}}{k_{\rm B}T}}. \tag{9}$$

The normalization factors $Z_{\rm S}$ and $Z_{\rm B}$ are the partition functions of the quantum harmonic oscillator and the bath, respectively. T refers to the temperature and $k_{\rm B}$ is the Boltzmann constant.

We now turn to the rotating frame and define two dimensionless amplitudes: $\bar{X}_1 = \cos(\omega t)X_1 - \sin\omega t X_2$, and $\bar{X}_2 = \sin\omega t X_1 + \cos(\omega t)X_2$. The equations of motion for the average values of $\bar{X}_1$ and $\bar{X}_2$ can be derived from Eqs. (7):

$$\langle\dot{\bar{X}}_1\rangle = \Delta\omega\langle\bar{X}_2\rangle - \frac{\gamma}{2}\langle\bar{X}_1\rangle, \tag{10}$$

$$\langle\dot{\bar{X}}_2\rangle = -\Delta\omega\langle\bar{X}_1\rangle - \frac{\gamma}{2}\langle\bar{X}_2\rangle - \frac{g}{2}, \tag{11}$$

where the terms that are oscillating at 2ω have been dropped, and $\Delta\omega = \omega_0 - \omega$ denotes the frequency detuning. In the regime of near resonance $\Delta\omega \ll \gamma$, the steady average of $\langle\bar{X}_1\rangle_{\rm s} = -2g\Delta\omega/[\gamma^2 + 4(\Delta\omega)^2]$ is much smaller that of $\langle\bar{X}_2\rangle_{\rm s} = -g\gamma/[\gamma^2 + 4(\Delta\omega)^2]$. This implies the average phase of the oscillator

$$\langle\phi\rangle = \arctan\left(\frac{\langle\bar{X}_1\rangle}{\langle\bar{X}_2\rangle}\right) \tag{12}$$

has a small steady-state phase shift from the resonant point $\langle\phi\rangle_{\rm r} = 0$. Furthermore, the frequency shift is nearly linear in the frequency detuning

$$\langle\phi\rangle_{\rm s} \approx \frac{\Delta\omega}{\gamma/2} \equiv T_2\Delta\omega, \tag{13}$$

where $T_2 = 2/\gamma$ is the coherence time of the harmonic oscillator. Therefore, the oscillator can be used as a sensor to measure the input frequency ω by monitoring the phase shift $\langle\phi\rangle_{\rm s}$.

The time evolution of the average phase $\langle\phi\rangle$, when the oscillator is operating near the resonant point, satisfies the equation

$$\langle\dot{\phi}\rangle \approx \Delta\omega - \frac{1}{T_2}\langle\phi\rangle. \tag{14}$$

Equations (13) and (14) show that longer coherence time T_2 results in higher sensitivity at the expense of slower response (narrower bandwidth).

Apart from the technique noise in the detection system, the phase measurement precision is ultimately limited by the fundamental uncertainty principle of quantum mechanics. In the oscillator model considered above, the phase shift $\langle\phi\rangle_{\rm s}$ cannot be measured with arbitrary precision. A key quantity characterizing how well we can determine the phase shift is the variance of the phase

$$\langle\Delta\phi\rangle_{\rm s} \approx \left|\frac{(\Delta\bar{X}_1)_{\rm s}}{\langle\bar{X}_2\rangle_{\rm s}}\right| = \frac{\sqrt{2\bar{n}+1}}{T_2 g}, \tag{15}$$

where $\bar{n}$ is the average quanta number in the frequency ω_0 and $(\Delta\bar{X}_1)_{\rm s}$ is the steady-state variance of $\bar{X}_1$. At absolute zero temperature,

$$\langle\Delta\phi\rangle_{\rm s} = \frac{1}{T_2 g} \tag{16}$$

gives the minimum phase uncertainty imposed by quantum fluctuations.

3. Feedback control and bandwidth improvement

The bandwidth of a quantum sensor can be analyzed with the method of transfer functions.[20] The model is presented in Fig. 1 with a proportional-integral controller (PI-controller), which is widely used in classic control field. The quantum sensor G, as discussed in the above section, representing an oscillator operating near its resonance point, is described by the transfer function according to Eq. (14):

$$G(s) = \frac{T_2}{1 + T_2 s}, \tag{17}$$

where s is the complex variable. The transfer function $G(s)$ relates the frequency detuning $\Delta\omega(s)$ to the phase shift signal $\phi(s)$, where $\Delta\omega(s)$ and $\phi(s)$ are the Laplace transformation of the corresponding time-domain signals.

In the open-loop operation condition, the detection of the signal $\Delta\omega$ can be described as follows. When the input frequency $\omega_{\rm i}$ is off-resonant from the resonant frequency of the oscillator G, the phase of the oscillator increases from zero value at the resonant point to a nonzero value ϕ. By monitoring the phase shift ϕ, the frequency detuning is deduced according to Eq. (13). Finally, equation (17) shows that the open-loop bandwidth is limited by the coherence time T_2.

Although long coherence time brings about high sensitivity [see Eq. (1)], it significantly limits the measurement bandwidth. Small bandwidth will limit practical applications of the quantum sensors. Fortunately, the problem of small open-loop bandwidth can be resolved by feedback control method.

In the close-loop system depicted in Fig. 1, a PI-controller is utilized for frequency $\omega_{\rm o}$ feedback, whose performance is characterized by two parameters: the proportional term $K_{\rm p}$ and the integral term $K_{\rm i}$. The central idea of the feedback is to keep the system in resonance by feedback controller. When the input frequency $\omega_{\rm i}$ deviates from the resonant point of the oscillator system ($\Delta\omega \neq 0$), the quantum sensor will generate nonzero phase output ϕ. According to the value of the nonzero phase, the PI-controller takes action and updates the frequency $\omega_{\rm o}$, which determines the new input detuning of G together with the input frequency $\omega_{\rm i}$. In this way, the feedback control system continuously monitors the phase of the oscillator, and maintains its value as close as possible to zero by adjusting the frequency detuning. As $\Delta\omega$ is close to zero with a feedback loop, $\omega_{\rm i}$ can be detected by the feedback frequency $\omega_{\rm o}$.

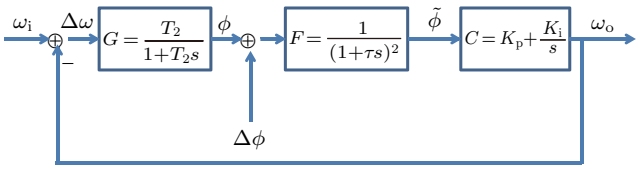

Fig. 1. The block diagram of the close-loop control of a quantum sensor system. The open-loop transfer function of the oscillator is denoted by G. A second order filter F with filter time constant τ is applied to suppress high frequency noise. A PI-controller C is used to adjust the output frequency $\omega_{\rm o}$ so as to trace the variation of the input frequency $\omega_{\rm i}$. The control parameter $K_{\rm p}$ represents the proportional term and $K_{\rm i}$ stands for the integral term. The quantum phase white noise $\Delta\phi$ will be a disturbance to the output of the PI-controller. Finally, the phase shift ϕ is the output of the sensor, followed by the high-frequency-noise-filtered phase shift $\tilde{\phi}$.

The principle of bandwidth improvement by feedback method is demonstrated in the following. In the absence of noise, the close-loop transfer function of the system is given by

$$\Phi_{\rm c}(s) = \frac{G(s)F(s)C(s)}{1+G(s)F(s)C(s)}, \tag{18}$$

related to input $\omega_{\rm i}(s)$ and output $\omega_{\rm o}(s)$. We first focus on the limit where the filter time constant $\tau \to 0$. In this limit, the transfer function $F(s) \approx 1$, and the close-loop transfer function

$$\Phi_{\rm c}(s) \approx \frac{C(s)}{1+G(s)C(s)}G(s) = A(s)G(s), \tag{19}$$

where

$$A(s) = C(s)/[1+C(s)G(s)]. \tag{20}$$

The function $A(s)$ is a key quantity that is responsible for increasing the bandwidth $\omega_{\rm B}$ from the open-loop one, $1/T_2$, to a much larger one.

The close-loop frequency response can be separated into two parts:

$$|\Phi_{\rm c}(j\omega)|^2 = \tilde{A}(\bar{\omega})A_{\bar{G}}(\bar{\omega}), \tag{21}$$

where

$$\tilde{A}(\bar{\omega}) = \frac{k_{\rm p}^2\bar{\omega}^4 + \left(k_{\rm p}^2+k_{\rm i}^2\right)\bar{\omega}^2 + k_{\rm i}^2}{\bar{\omega}^4 + \left[-2k_{\rm i}+\left(1+k_{\rm p}\right)^2\right]\bar{\omega}^2 + k_{\rm i}^2}, \tag{22}$$

$$A_{\bar{G}}(\bar{\omega}) = \frac{1}{1+\bar{\omega}^2}. \tag{23}$$

Here, we have introduced three dimensionless parameters: $\bar{\omega} = \omega T_2$, $k_{\rm p} = K_{\rm p}T_2$ and $k_{\rm i} = K_{\rm i}T_2^2$.

In the region $k_{\rm i} < (1+k_{\rm p})^2/2$, the function $\tilde{A}(\bar{\omega})$ can be analyzed in the log-log coordinate, and the numerator and denominator of $\tilde{A}(\bar{\omega})$ can be well approximated by several broken lines representing terms proportional to $\bar{\omega}^4$, $\bar{\omega}^2$ and the constant terms $k_{\rm i}^2$ as shown in Fig. 2. There are four boundary points characterizing the dominant contributions of constant, $\bar{\omega}^2$, $\bar{\omega}^4$ terms in different $\bar{\omega}$ regions:

$$\bar{\omega}_2^{(\rm n)} = \frac{k_{\rm i}}{\sqrt{k_{\rm p}^2+k_{\rm i}^2}}, \tag{24}$$

$$\bar{\omega}_{24}^{(\rm n)} = \frac{\sqrt{k_{\rm p}^2+k_{\rm i}^2}}{k_{\rm p}}, \tag{25}$$

$$\bar{\omega}_2^{(\rm d)} = \frac{k_{\rm i}}{\sqrt{-2k_{\rm i}+\left(1+k_{\rm p}\right)^2}}, \tag{26}$$

$$\bar{\omega}_{24}^{(\rm d)} = \sqrt{-2k_{\rm i}+\left(1+k_{\rm p}\right)^2}, \tag{27}$$

where $\bar{\omega}_2^{(\rm n)}$ is the cross point between $k_{\rm i}^2$ and the $\bar{\omega}^2$ terms in the numerator, and $\bar{\omega}_{24}^{(\rm n)}$ is the cross point between the $\bar{\omega}^2$ terms and the $\bar{\omega}^4$ terms in the numerator. The $\bar{\omega}_2^{(\rm d)}$ and $\bar{\omega}_{24}^{(\rm d)}$ are corresponding cross points in the denominator of $\tilde{A}(\bar{\omega})$. In the regimes $k_{\rm p} \gg k_{\rm i}$ and $k_{\rm p} \gg 1$,

$$\bar{\omega}_2^{(\rm n)} \approx \bar{\omega}_2^{(\rm d)} \approx \frac{k_{\rm i}}{k_{\rm p}}, \tag{28}$$

$$\bar{\omega}_{24}^{(\rm n)} \approx 1, \tag{29}$$

$$\bar{\omega}_{24}^{(\rm d)} \approx k_{\rm p}. \tag{30}$$

Under this condition, the numerator terms $A^{(\rm n)}(\bar{\omega})$, the denominator term $A^{(\rm d)}(\bar{\omega})$ and $\tilde{A}(\bar{\omega})$ are well approximated by Fig. 2. The close-loop frequency response $|\Phi_{\rm c}(j\omega)|^2$ is the product of $\tilde{A}(\bar{\omega})$ and $A_{\bar{G}}(\bar{\omega})$. As demonstrated by Fig. 2, the bandwidth has been increased from the open-loop value $\bar{\omega}_{\rm B} = 1$ to the close-loop value $\bar{\omega}_{\rm B} = k_{\rm p}$.

Figure 2 shows that the close-loop frequency response is maximum in the zero frequency and decreases with $\bar{\omega}$ when $k_{\rm i} \ll k_{\rm p}$. As $k_{\rm i}$ grows and exceeds a critical point

$$k_{\rm i}^{\rm c} = k_{\rm p} + 1/2, \tag{31}$$

the close-loop frequency response will exhibit resonant behavior. In this case it acquires a maximum value at some positive frequency $\bar{\omega}$ as demonstrated in Fig. 3. This resonant behavior corresponds to the condition that

$$\frac{\partial}{\partial k_{\rm i}}|\Phi_{\rm c}(j\omega)|^2 = 0 \tag{32}$$

has a positive frequency solution.

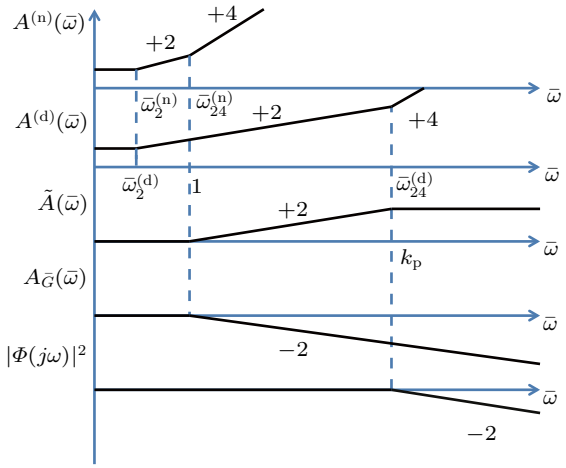

Fig. 2. Schematic diagram of bandwidth improvement by PID feedback. These curves are depicted in the log–log coordinates, where $A^{(n)}(\bar{\omega})$ and $A^{(d)}(\bar{\omega})$ represent the numerator and denominator of $\tilde{A}(\bar{\omega})$, respectively. The numbers $+2$ and $+4$ indicate that the terms proportional to $\bar{\omega}^2$ and $\bar{\omega}^4$ are dominant in those frequency intervals. The number -2 indicates that the functions decay as $1/\bar{\omega}^2$ in those frequency intervals.

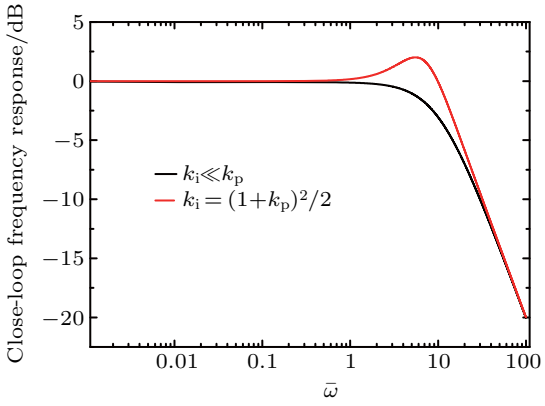

Fig. 3. Demonstrations of the resonant and non-resonant behaviors of the close-loop frequency responses $A_{\rm close}(\omega)$. The black curve represent the regime $k_{\rm i} \ll k_{\rm p}$, while the red curve present resonant behavior with $k_{\rm i} > k_{\rm i}^{\rm c}$. In this graph, $k_{\rm p} = 100$ and $k_{\rm i} = (1+k_{\rm p})^2$.

The above discussion shows that the bandwidth of the close-loop system can be improved without a limit by increasing $k_{\rm p}$, keeping $k_{\rm i} \ll k_{\rm p}$ at the same time. When finite filter time constant τ is taken into consideration, the close-loop bandwidth will be ultimately limited by τ. However, in practical applications the filter time constant τ can be adjusted to a value such that $1/\tau \gg \omega_{\rm B} \approx k_{\rm p}/T_2$. In this case, the bandwidth can still be improved by the method we discussed above. Figure 4 shows that when the bandwidth $\omega_{\rm B}$ is much smaller than $1/\tau$, $\omega_{\rm B}$ is still determined by $k_{\rm p}$. The filter F begins to take effect at frequency $1/\tau$ and suppresses high-frequency noise.

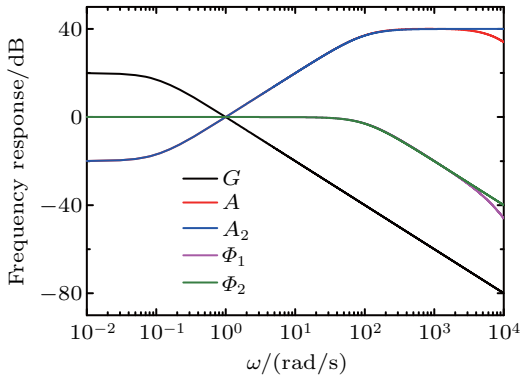

Fig. 4. Comparisons of frequency responses with filter F present or not. The black curve represents the frequency response of the open-loop system G. The pink and green curves describe the close-loop frequency responses of $\Phi_1(s) = CGF/(1+CGF)$ and $\Phi_2(s) = CG/(1+CG)$ when the filter F is present or not, respectively. The blue and red curves correspond to the frequency responses of $A_1(s) = CF/(1+CGF)$ and $A_2(s) = A(s)$, respectively. The parameters used in this graph are $T_2 = 10$ s, $\tau = 10^{-4}$ s, $k_{\rm p} = 1000$ and $k_{\rm i} = 100$.

4. Competition between bandwidth and sensitivity

As discussed above, the feedback method indeed improves the bandwidth of the sensor, when PI parameters are properly chosen. In this section, we consider the effect of the noise on the performance of the quantum sensor. The noise under consideration is assumed to be due to purely quantum mechanical origin, which roots in the quantum characteristic of the sensor, as given by Eq. (16).

The noise transfer in the closed-loop sensor system is shown in Fig. 5(a). The noise will cause an output frequency fluctuation $\omega_{\rm n}(s)$ in the PI controller, thus limiting the sensitivity of the sensor. The transfer function relating $\omega_{\rm n}(s)$ to $\Delta\phi(s)$ is

$$\Phi_{\rm n}(s) = \frac{\omega_{\rm n}(s)}{\Delta\phi(s)} = \frac{CF}{1+CGF}. \tag{33}$$

The output frequency fluctuation $\omega_{\rm n}(t)$ thus has a power spectral density (PSD)[21]

$$S_{\rm n}(\omega) = |\Phi_{\rm n}(j\omega)|^2 S_0, \tag{34}$$

where S_0 is the power spectral density of the input phase noise. The magnitude of S_0 can be estimated as follows. The Wiener–Khinchin theorem shows that the variance of the phase white noise equals the integral of the corresponding PSD over the frequency domain. Thus we can estimate S_0 by

$$S_0 = \frac{1}{(T_2 g)^2}\frac{1}{B}, \tag{35}$$

where B refers to the largest bandwidth in the measurement system, and can be taken as $1/\tau$, since τ is the minimum time constant under consideration. Then $S_{\rm n}(\omega)$ has the form

$$S_{\rm n}(\omega) = |\Phi_{\rm n}(j\omega)|^2 \frac{\tau}{(T_2 g)^2}. \tag{36}$$

The plot of $S_n^{1/2}(\omega)$ versus the dimensionless angular frequency $\bar{\omega}$ is depicted in Fig. 5(b) with different PI parameters. As the proportional constant K_p increases, the noise is further amplified by the feedback loop. The increased noise power will degrade the performance of the sensor, because the signal to be detected is determined by the frequency increment $\Delta\omega$ and ω_n will contaminates the output of ω_o. This reveals the competitive relationship between bandwidth and sensitivity, since increasing K_p will improve the bandwidth and degrade the sensitivity inevitably at the same time.

The competitive relationship between bandwidth and sensitivity can also be perceived qualitatively and visually. Equation (33) shows that the transfer function $\Phi_n(s)$ is identical to $\Phi_c(s)/G(s)$, and Fig. 4 indicates that the function of $\Phi_n(s)$ is to increase the bandwidth of the sensor from the open-loop value $1/T_2$ to the closed-loop value k_p/T_2. For the sake of achieving large bandwidth, the frequency response of $\Phi_n(s)$ must compensate for the drop of $G(s)$ when $\omega > 1/T_2$, which indicates the amplification of the noise with frequency in this frequency range. Therefore, the sensitivity of the sensor is further reduced when larger k_p is chosen.

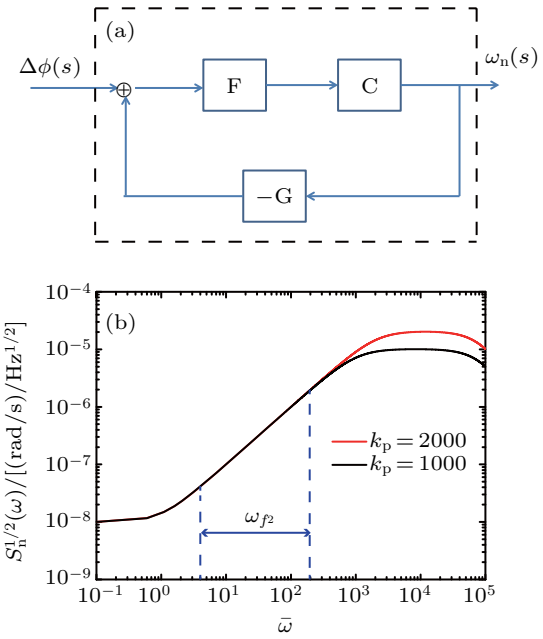

Fig. 5. (a) The block diagram of the noise transfer. The noise $\Delta\phi(s)$, which is here the Laplace transformation of $\Delta\phi(t)$, causes a output frequency fluctuation in the PI controller, as represented by $\omega_n(s)$ in the above diagram. (b) The power spectral density $S_n^{1/2}(\omega)$ of the noise output $\omega_n(t)$. The red curve is depicted with $k_p = 2000$, which is twice over that of the black one. Other parameters used are $k_i = 100$, $T_2 = 10$ s, $\tau/T_2 = 10^{-5}$, and $T_2 g = 10^3$.

Another point to be emphasized is that the original quantum phase noise $\Delta\phi$ can influence the sensor's sensitivity in a non-white form by means of frequency output fluctuation $\omega_n(t)$, since the sensor's sensitivity is determined by $S_n^{1/2}(\omega)$. As shown in Fig. 5, $S_n^{1/2}(\omega)$ has a positive slope 1, which indicates a f^2 noise contribution in the noise spectrum $S_n(\omega)$. In higher frequency intervals, the noise spectrum $S_n^{1/2}(\omega)$ becomes more complex, and is not white noise as well.

5. Conclusions

In summary, we have investigated the relationship between bandwidth and sensitivity of a quantum sensor based on the transfer function method. The results indicate that the bandwidth of sensor are greatly increased by feedback when choose proper PI parameters. The proportional term K_p is the key parameter in improving bandwidth. Unfortunately, the quantum noise inherent to the quantum sensor system will be further amplified when larger bandwidth is achieved. The bandwidth and sensitivity are two competing performance parameters. Therefore, there must be a trade-off between bandwidth and sensitivity in applying the quantum sensor into practical application. In addition, an original quantum white noise may present itself in form of f^2-noise due to the feedback control.

References

[1] Allred J C, Lyman R N, Kornack T W and Romalis M V 2002 *Phys. Rev. Lett.* **89** 130801

[2] Kominis I, Kornac T, Allred J and Romalis M V 2003 *Nature* **422** 596

[3] Savukov I M, Seltzer S J, Romalis M V and Sauer K L 2005 *Phys. Rev. Lett.* **95** 063004

[4] Budker D and Kimball D F J 2013 *Optical Magnetometry* (Cambridge: Cambridge University Press)

[5] Maiwald R, Leibfried D, Britton J, Bergquist J C, Leuchs G and Wineland D J 2009 *Nat. Phys.* **5** 551

[6] Biercuk M J, Uys H, Britton J W, VanDevender A P and Bollinger J J 2010 *Nat. Nanotechnol.* **5** 646

[7] Brownnutt M, Kumph M, Rabl P and Blatt R 2015 *Rev. Mod. Phys.* **87** 1419

[8] Balasubramanian G, Chan I Y, Kolesov R *et al.* 2008 *Nature* **455** 648

[9] Taylor J, Cappellaro P, Childress L, Jiang L, Budker D, Hemmer P, Yacoby A, Walsworth R and Lukin M 2008 *Nat. Phys.* **4** 810

[10] Ledbetter M P, Jensen K, Fischer R, Jarmola A and Budker D 2012 *Phys. Rev. A* **86** 052116

[11] Wolf T, Neumann P, Nakamura K, Sumiya H, Ohshima T, Isoya J and Wrachtrup J 2015 *Phys. Rev. X* **5** 041001

[12] Giovannetti V, Lloyd S and Maccone L 2004 *Science* **306** 1330

[13] Leibfried D, Barrett M D, Schaetz T, Britton J, Chiaverini J, Itano W M, Jost J D, Langer C and Wineland D J 2004 *Science* **304** 1476

[14] Bollinger J J, Itano W M, Wineland D J and Heinzen D J 1996 *Phys. Rev. A* **54** R4649

[15] Caves C M 1981 *Phys. Rev. D* **23** 1693

[16] Schnabel R, Mavalvala N, McClelland D E and Lam P K 2010 *Nat. Commun.* **1** 121

[17] Abadie J, Abbott B, Abbott R, Abbott T, Abernathy M, Adams C, Adhikari R, Akeldt C, Allen B, Allen G *et al.* 2011 *Nat. Phys.* **7** 962

[18] Degen C L, Reinhard F and Cappellaro P 2017 *Rev. Mod. Phys.* **89** 035002

[19] Scully M O and Zubairy M S 1997 *Quantum Optics* (Cambridge: Cambridge University Press)

[20] Ogata K 2009 *Modern Control Engineering* (Upper Saddle River NJ: Prentice Hall)

[21] Davenport W B, Root W L *et al.* 1958 *An introduction to the Theory of Random Signals and Noise* (New York: McGraw-Hill) Vol. 159